Decreased Subunit Stability as a Novel Mechanism for Potassium Current Impairment by a KCNQ2 C Terminus Mutation Causing Benign Familial Neonatal Convulsions*

Maria Virginia Soldovieri[‡1], Pasqualina Castaldo[‡§1], Luisa Iodice[¶], Francesco Miceli[‡], Vincenzo Barrese[‡], Giulia Bellini[‖**], Emanuele Miraglia del Giudice[**], Antonio Pascotto[‖], Stefano Bonatti[¶], Lucio Annunziato[‡], and Maurizio Taglialatela[‡‡‡2]

From the ‡Division of Pharmacology, Department of Neuroscience, and ¶Department of Biochemistry and Medical Biotechnology, University of Naples Federico II, 80131 Naples, the ‖Chair of Child Neuropsychiatry and **Department of Pediatrics, Second University of Naples, 80131 Naples, the §Department of Neuroscience, University of Ancona, 60121 Ancona, and the ‡‡Department of Health Sciences, University of Molise, 86100 Campobasso, Italy

KCNQ2 and KCNQ3 K$^+$ channel subunits underlie the muscarinic-regulated K$^+$ current (I_{KM}), a widespread regulator of neuronal excitability. Mutations in KCNQ2- or KCNQ3-encoding genes cause benign familiar neonatal convulsions (BFNCs), a rare autosomal-dominant idiopathic epilepsy of the newborn. In the present study, we have investigated, by means of electrophysiological, biochemical, and immunocytochemical techniques in transiently transfected cells, the consequences prompted by a BFNC-causing 1-bp deletion (2043ΔT) in the *KCNQ2* gene; this frameshift mutation caused the substitution of the last 163 amino acids of the KCNQ2 C terminus and the extension of the subunit by additional 56 residues. The 2043ΔT mutation abolished voltage-gated K$^+$ currents produced upon homomeric expression of KCNQ2 subunits, dramatically reduced the steady-state cellular levels of KCNQ2 subunits, and prevented their delivery to the plasma membrane. Metabolic labeling experiments revealed that mutant KCNQ2 subunits underwent faster degradation; 10-h treatment with the proteasomal inhibitor MG132 (20 μM) at least partially reversed such enhanced degradation. Co-expression with KCNQ3 subunits reduced the degradation rate of mutant KCNQ2 subunits and led to their expression on the plasma membrane. Finally, co-expression of KCNQ2 2043ΔT together with KCNQ3 subunits generated functional voltage-gated K$^+$ currents having pharmacological and biophysical properties of heteromeric channels. Collectively, the present results suggest that mutation-induced reduced stability of KCNQ2 subunits may cause epilepsy in neonates.

Voltage-gated potassium (K$^+$) channels represent the most heterogeneous class of ion channels with respect to kinetic properties, regulation, and pharmacology (1). In neuronal cells, voltage-gated K$^+$ channels regulate excitability by controlling action potential duration, subthreshold electrical properties, and responsiveness to synaptic inputs.

Among neuronal K$^+$ currents, the muscarinic-regulated K$^+$ current (I_{KM})[3] activates slowly during long-lasting depolarizing inputs and repolarizes the neuronal membrane back toward resting membrane potential (2), thus limiting repetitive firing and causing spike-frequency adaptation (3). I_{KM} is strongly and reversibly suppressed by activation of phospholipase C-linked G-protein-coupled receptors; receptor-dependent regulation of I_{KM} is a primary mechanism by which neurotransmitters and neuromodulators control neuronal excitability (4). Heteromeric assembly of K$^+$ channel subunits encoded by members of the KCNQ subfamily, namely KCNQ2 (Q2) and KCNQ3 (Q3), seems to represent the main molecular substrates of I_{KM} (5, 6), although KCNQ4 (7) and KCNQ5 (8, 9) may also participate. Interestingly, drug-induced enhancement of I_{KM}, by suppressing excessive neuronal activity, exerts potent anticonvulsant and analgesic effects, thus revealing a novel role for this K$^+$ current as a primary pharmacological target for epilepsy and pain therapy (3).

The fundamental role played by I_{KM} in human epilepsy has received strong genetic support upon discovery that mutations in either *Q2* (10, 11) or *Q3* (12) are responsible for benign familiar neonatal convulsions (BFNCs; MIM 121200), a rare autosomal-dominant idiopathic epilepsy of the newborn. This disease is characterized by the occurrence of multifocal or generalized tonic-clonic convulsions starting around day 3 of post-natal life and spontaneously disappearing after a few weeks or months (13). Although neurocognitive development is normal in most BFNC-affected individuals, 10–15% of them will experience convulsive episodes or altered EEG activity later in life (14). Despite this crucial pathogenetic role for BFNC, no genetic association has been detected between *Q2* (15) or *Q3* (16) allelic variants and the more conventional idiopathic human epilepsies.

Until today, about thirty *Q2* and three *Q3* mutations have been discovered in families affected by BFNC (17). Those mutations whose functional consequences have been investigated (11, 18–20) cause a small (<25%) reduction in the maximal current carried by the Q2/Q3 channels; only two *Q2* mutations caused a more dramatic current reduction, consistent with a dominant-negative effect (17, 21). A large fraction of BFNC-causing mutations in *Q2* are represented by insertions or deletions leading to changes in the primary sequence of the long cytosolic C terminus, where relevant sites have been detected for func-

[3] The abbreviations used are: I_{KM}, muscarinic-regulated K$^+$ current; BFNC, benign familiar neonatal convulsion; CTS, centrotemporal spikes; EGFP, enhanced green fluorescent protein; CHO cells, Chinese hamster ovary cells; Huh cells, Human hepatoma cells; ER, endoplasmic reticulum; NEM, *N*-ethylmaleimide; TEA, tetraethylammonium; hERG1, *Ether-a-gogo-Related* Gene-1; pF, picofarad(s); HA, hemagglutinin.

tional regulation. In fact, specific sequences within this region (the so-called "subunit interaction domain" or *sid*) (22) dictate the specificity of KCNQ subunit assembly and provide sites where other signaling proteins such as calmodulin (23, 24) and protein kinases and kinase-anchoring proteins (25) interact with KCNQ subunits and modulate channel activity.

Members of our research team have recently described a *Q2* mutation in a patient with BFNC who later showed an electroencephalographic trait characterized by centrotemporal spikes at the age of 3 years; the mutation is an heterozygous 1-bp deletion (2043ΔT) in *Q2* exon 16, leading to the substitution of the C-terminal 163 amino acids and to the extension of the Q2 subunit by additional 56 residues. Electrophysiological studies in *Xenopus* oocytes and transiently transfected mammalian cells revealed that K$^+$ channel subunits carrying the 2043ΔT mutation did not give rise to functional homomeric channels (26).

In the present study, we have investigated the molecular mechanisms responsible for the lack of functional voltage-gated K$^+$ channel observed upon expression of Q2 2043ΔT mutant subunits by means of a combined biochemical, immunocytochemical, and electrophysiological approach in transiently transfected mammalian cells. The results obtained show that the 2043ΔT mutation reduced the steady-state cellular levels of Q2 subunits, consequent to a marked enhancement of their degradation. The 2043ΔT mutation-induced enhanced degradation of Q2 subunits seems to occur via the proteasomal disposition pathway and leads to a drastic reduction of mutant subunits delivery to the plasma membrane. Furthermore, co-expression with Q3 subunits at least partially reversed the enhanced degradation caused by the 2043ΔT mutation in *Q2*, leading to the expression of functional heteromeric channels composed of Q2 2043ΔT and Q3 subunits in the plasma membrane. Collectively, the present results suggest that mutation-induced enhanced degradation of Q2 subunits may represent a novel molecular mechanism causing epilepsy in neonates.

EXPERIMENTAL PROCEDURES

Mutagenesis and Heterologous Expression of KCNQ Subunits—Q2 mutations were engineered in human Q2 cDNA (pTLN-Q2) (11) by sequence overlap extension PCR with the *Pfu* DNA polymerase, as described (25). The original pTLN-Q2 construct was modified to include additional 94 bp from the 3′UTR of exon 16 (26). To create fusion proteins between Q2 and enhanced green fluorescent protein (EGFP), the cDNA encoding for Q2 was modified either at the 5′UTR or at the 3′UTR, as following. Briefly, to place the EGFP before the N terminus of the Q2 subunit (EGFP-Q2), an HindIII-NotI cassette of Q2 was generated, encoding for the N-terminal region of the subunit; 7 glutamine (Q) residues were introduced by PCR immediately before the translation start codon (ATG) to increase protein flexibility, using the following oligonucleotides: (forward): 5′-agctcaagcttccagcagcagcagcagcagcagatggtgcagaagtcgcgcaacggcggcgtatacc-3′; (reverse): 5′-agccgcgcggccgctccagcac-3′.

To place the EGFP after the C terminus of the Q2 subunit (Q2-EGFP), it was necessary modify the 3′UTR of Q2 cDNA to eliminate the natural stop codon (TGA) and to introduce the 7 Q linker. These modifications were made in a Q2 C-terminal cassette (SalI-EcoRI) by PCR using the following oligonucleotides: (forward): 5′-gagcatgtcgacaggcacggc-3′; (reverse): 5′-ccggtgaattcctgctgctgctgctgctgctgcttcctgggcccggcccagcccacgtcaccaaagg-3′.

PCR products were cloned in a TOPO TA cloning vector (Invitrogen) and introduced into the pTLN-Q2 construct using the HindIII-NotI and SalI-EcoRI restriction enzymes, respectively. These Q2 constructs

(modified at their N- or C-terminal regions) were excised using the HindIII-EcoRI restriction enzymes and cloned in the EGFP-C2 and EGFP-N2 vectors from Clontech (Palo Alto, CA), respectively. C-terminal BFNC mutations were introduced by cloning in the EGFP-Q2 fusion protein construct using the BSTXI-EcoRI restriction enzymes from previously generated Q2–2043ΔT and Q2–2513ΔG constructs (24). DNA sequences were verified using an ABI PRISM 310 sequencing apparatus (Applied Biosystems, Foster City, CA). The chimeric constructs in which an hemagglutinin epitope (HA epitope) was inserted into Q2 subunits were engineered by cloning a NotI/PmlI fragment removed from a pTLN-Q2/HA into wtEGFP-Q2 and EGFP-Q2 2043ΔT constructs (20).

For mammalian cell expression, cDNAs were transfected into Chinese hamster ovary (CHO) and human hepatoma (Huh-7) cells using Lipofectamine 2000 (Invitrogen), according to the manufacturer protocols. CHO cells were grown in Dulbecco's modified Eagle's medium containing 10% fetal bovine serum, nonessential amino acids (0.1 mM), penicillin (50 units/ml), and streptomycin (50 μg/ml), in an humidified atmosphere at 37 °C with 5% CO_2 in 100-mm plastic Petri dishes. For electrophysiological experiments, the cells were seeded on glass coverslips (Carolina Biological Supply Co., Burlington, NC). All the experiments were performed 1–2 days after transfection.

Cell-surface Biotinylation and Western Blotting—Channel subunits in total lysates from CHO cells were analyzed by Western blotting as described (27). Membrane strips were incubated overnight at 4 °C with mouse monoclonal anti-EGFP antibodies (1:1000 dilution) from Clontech or goat polyclonal anti-KCNQ2 antibodies (1:200 dilution) from Santa Cruz Biotechnology (sc-7792 and sc-7793, Santa Cruz, CA); reactive bands were detected by chemiluminescence (SuperSignal, Pierce) on a ChemiDoc station (Bio-Rad). Images were captured, stored, and analyzed with the Quantity One analysis software (Bio-Rad). An anti-α-tubulin antibody (Sigma, dilution 1:5000) was used to check for equal protein loading. When necessary, plasma membrane expression of wild-type and mutant EGFP-Q2 subunits in CHO cells was investigated by surface biotinylation of membrane proteins in intact transfected cells using Sulfo-NHS-LC-Biotin (Pierce), a cell-membrane impermeable reagent, following the manufacturer's protocol. Following cell biotinylation and lysis, fraction of cell lysates were reacted with ImmunoPure immobilized streptavidin beads (Pierce) and analyzed by Western blotting on 6% SDS-PAGE gels. To confirm that the biotinylation reagent did not leak into the cell and label intracellular proteins, we stripped and reprobed the same blots with mouse anti-α-tubulin antibodies (1:2000 dilution).

*Metabolic Labeling, Preparation of Cell Extracts, Immunoprecipitation, SDS-PAGE, and Quantitative Analysis*—All of the procedures were performed as described previously (28). To quantify the relative amounts of immunolabeled or radioactively labeled bands after immunoblotting or pulse-chase labeling, respectively, the autoradiographic films were analyzed with the Image program (NIMH, National Institutes of Health, Bethesda, MD).

Immunofluorescence Analysis—CHO and Huh-7 cells were grown on glass coverslips and manipulated for indirect immunofluorescence as previously described (29). Cells were observed under an Axiophot microscope or with an LSM 510 confocal laser scanning microscope (Carl Zeiss, Jena, Germany).

In the experiments shown in Fig. 7, to enhance detection of plasma membrane-specific signals related to KCNQ2 subunits in non-permeabilized cells, specimens were first incubated with a primary mouse monoclonal antibody anti-HA (Roche Applied Science, 1:200 dilution), then with a secondary polyclonal rabbit anti-mouse antibody (Vector

FIGURE 1. **Functional characterization of fusion proteins between EGFP and KCNQ2 subunits.** *A*, patch clamp recordings from CHO cells transfected with the plasmids encoding for EGFP alone, EGFP plus Q2, or EGFP-Q2 or Q2-EGFP fusion proteins. Holding potential: −80 mV; step potentials from −80 to +20 mV, in 10 mV steps; return potential: −60 mV (the protocol is shown in the *inset*). *B*, quantification of the current densities recorded from the four experimental groups. In this and the following figures, current densities were calculated by dividing the peak current at the end of the +20 mV pulse by the membrane capacitance in each recorded cell. Each *bar* is the mean ± S.E. of 12–26 cells recorded from at least three different transfections. *C*, conductance-voltage curves for the homomeric channels composed of Q2, EGFP-Q2, and Q2-EGFP subunits (see "Experimental Procedures" for details); *D*, Western blot analysis on total cell lysates from control CHO cells, or from cells transfected with the plasmids encoding for Q2, EGFP, or EGFP-Q2. Expression of fusion constructs with EGFP was detected using a monoclonal antibody against EGFP. The image shown is representative of five experiments, each giving similar results. Note the faint expression of smaller MW bands (<45 kDa), most likely related to EGFP, in cell lysates from EGFP-Q2-tranfected cells. The *lower image* in this panel shows the same blot stripped and reprobed with anti-α-tubulin antibodies, as indicated.
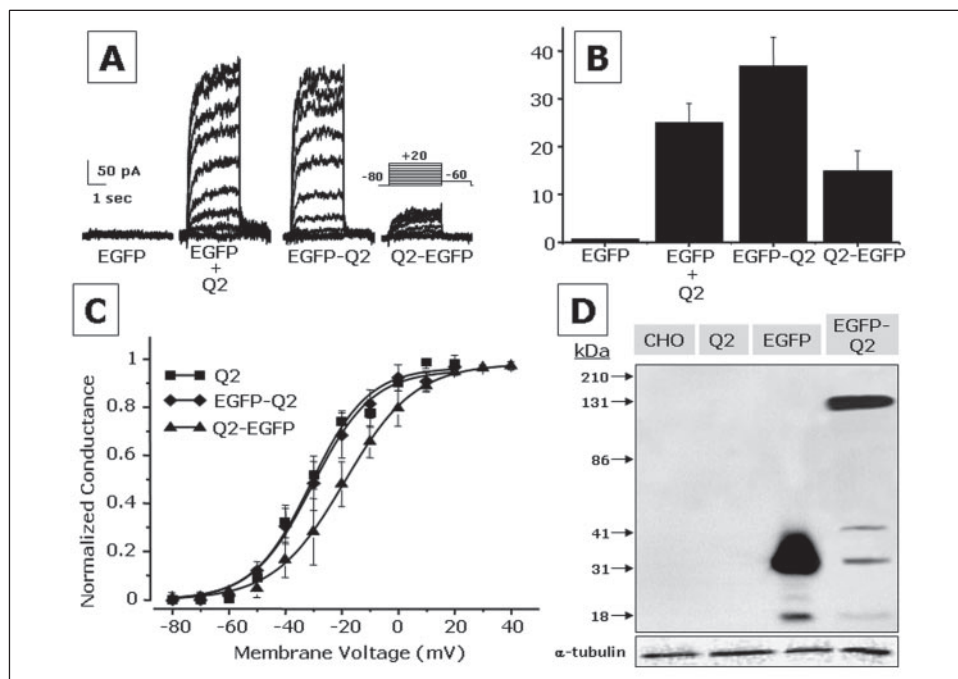
Laboratories Inc., Burlingame, CA, 1:200 dilution), and finally with a tertiary Texas red-conjugated polyclonal goat anti-rabbit antibody (the Jackson ImmunoResearch, West Groove, PA, 1:200 dilution).

Electrophysiology—Currents from CHO cells were recorded at room temperature (20–22 °C) using a commercially available amplifier (Axopatch 200A, Axon Instruments, Foster City, CA). The whole cell configuration of the patch clamp technique was adopted using glass micropipettes of 3–5 MΩ resistance. No compensation was performed for pipette resistance and cell capacitance. The cells were perfused with an extracellular solution containing (in mM): 138 NaCl, 2 CaCl$_2$, 5.4 KCl, 1 MgCl$_2$, 10 glucose, and 10 HEPES, pH 7.4, with NaOH. The pipettes were filled with an intracellular solution of the following composition (in mM): 140 KCl, 2 MgCl$_2$, 10 EGTA, 10 HEPES, 5 Mg-ATP, 0.25 mM cAMP, pH 7.3–7.4, with KOH. The pCLAMP (version 6.0.4, Axon Instruments) software was used for data acquisition and analysis.

Data Analysis and Statistics—Conductance-voltage curves were generated by a voltage protocol in which the cell was first depolarized for 3 s to voltages from −70 mV to +40 mV, in 10-mV increments, followed a 750-ms pulse to a constant voltage of 0 mV (or −60 mV in some experiments). The currents recorded at the beginning of the second pulse were measured, normalized to the maximal value, and expressed as a function of the preceding voltages. The data were fit to a Boltzmann distribution of the following form: $y = max/(1 + \exp(V_{1/2} - V)/k)$, where V is the test potential, $V_{1/2}$ the half-activation potentials, k the slope, and 'max' the maximal amplitude for the Boltzmann distribution. For each recorded cells, the capacitance of the membrane was calculated according to the following equation: $C_m = \tau_c \cdot I_o/\Delta E_m(1 - I_\infty/I_o)$, where C_m is membrane capacitance, τ_c is the time constant of the membrane capacitance, I_o is maximum capacitance current value, ΔE_m is the amplitude of the voltage step, and I_∞ is the amplitude of the steady-state current. Current amplitude data are expressed as current densities (picoamperes/picofarads or pA/pF). Data are expressed as the Mean ± S.E. Statistically significant differences between the groups were evaluated with the Student's *t* test ($p < 0.05$).

RESULTS

Functional Characterization of Fusion Proteins between EGFP and KCNQ2 Subunits—Fig. 1*A* shows representative traces of macroscopic K$^+$ current recordings from CHO cells transfected with the cDNA encoding for fusion proteins in which the EGFP was placed at the N terminus (EGFP-Q2), or at the C terminus (Q2-EGFP) of the Q2 subunit, as compared with those of CHO cells transfected with the plasmid encoding for EGFP (EGFP) or co-transfected with EGFP and Q2 plasmids (EGFP + Q2). Both fusion constructs gave rise to K$^+$ currents significantly larger than EGFP-transfected control cells, although the currents recorded from Q2-EGFP-trasfected cells were smaller than those recorded from EGFP-Q2-transfected cells (Fig. 1*B*). Analysis of the gating properties of homomeric channels composed of these fusion proteins revealed that the midpoint potentials ($V_{1/2}$) and the slopes (k) of the activation curves were, respectively, −29.3 ± 1 mV and 11.4 ± 0.8 mV/e-fold for Q2 ($n = 11$), −33.2 ± 0.5 mV and 9.3 ± 0.4 mV/e-fold for EGFP-Q2 ($n = 9$), and −19.0 ± 0.4 mV and 12.4 ± 0.3 mV/e-fold for Q2-EGFP ($n = 5$) (Fig. 1*C*). Therefore, when compared with homomeric Q2 channels, homomeric channels composed of Q2-EGFP subunits display a statistically significant ($p < 0.05$) 10-mV positive shift in the voltage dependence of activation; by contrast, no gating differences were apparent between homomeric EGFP-Q2 and Q2 channels.

Fig. 1*D* shows the results of a Western blot experiment performed 48 h post-transfection on total cell lysates from control CHO cells, or from cells transfected with the plasmids encoding for Q2, EGFP, or EGFP-Q2. Expression of EGFP was detected using a monoclonal antibody against EGFP; this antibody revealed a main band in EGFP-Q2-tranfected cells having a molecular mass (~130 kDa) that closely matched that predicted for the EGFP-Q2 fusion protein. Densitometric quantification of this band in untransfected, Q2-transfected, and EGFP-transfected CHO cells gave values of 2 ± 1%, 1 ± 1%, and 4 ± 2% of that obtained in EGFP-Q2-transfected cells ($n = 3$). A protein band having a similar molecular mass of ~130 kDa was also detected in cell lysates from EGFP-Q2-transfected cells when antibodies against N- or C-terminal epitopes of Q2 subunits were used (data not shown).

FIGURE 2. **Electrophysiological analysis of C-terminal BFNC-causing mutations expressed in homomeric configuration.** *A*, patch clamp recordings from CHO cells transfected with the plasmids encoding for EGFP-Q2, EGFP-Q2 2043ΔT, or EGFP-Q2 2513ΔG. Holding potential: −80 mV; step potentials from −80 to +20 mV, in 20-mV steps; return potential: 0 mV (the protocol is shown at the *bottom*). *B*, quantification of the current densities recorded from the four experimental groups. Each *bar* is the mean ± S.E. of 12–26 cells recorded from at least three different transfections.
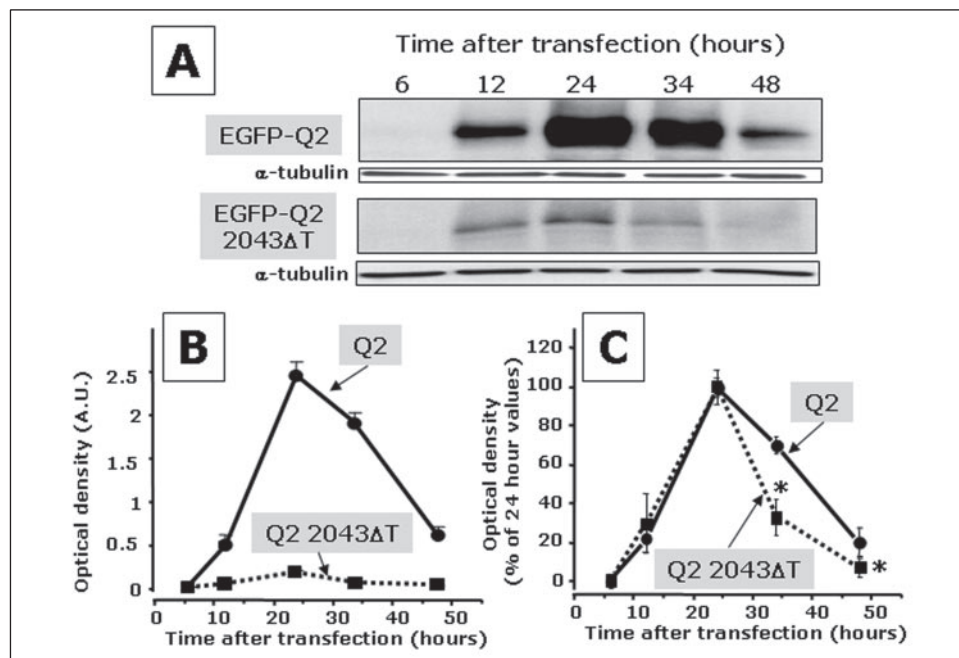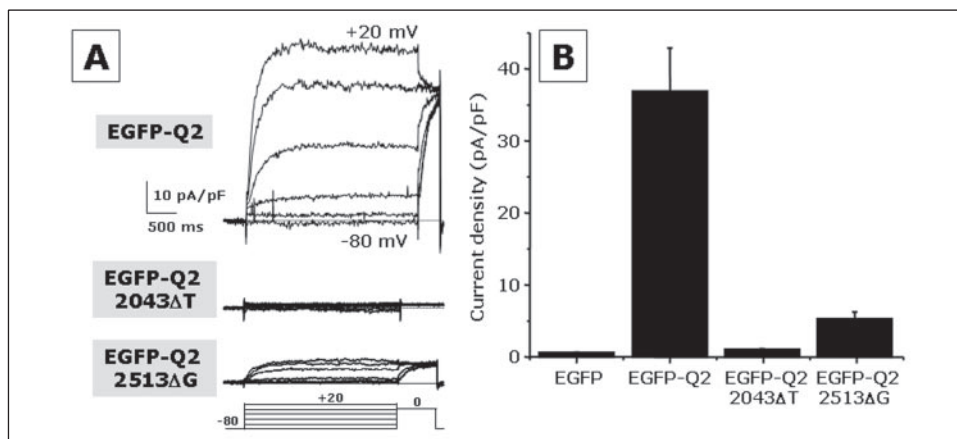
FIGURE 3. **Biochemical analysis of the 2043ΔT BFNC-causing mutations expressed in homomeric configuration.** *A*, time-course analysis (6, 12, 24, 34, and 48 h post-transfection) of EGFP-Q2 and EGFP-Q2 2043ΔT protein expression by Western blots on total cell lysates from CHO cells; fusion proteins were detected using an anti-EGFP monoclonal antibody. The *panels* at the *bottom* of each *image* show the expression, on the same filters, of the intracellular protein α-tubulin, used as an internal standard for equal protein loading. *B*, quantification of wild-type EGFP-Q2 (*filled circles*) and mutant EGFP-Q2 2043ΔT (*filled squares*) protein expression data of *A*. The data are expressed as arbitrary units (*A.U.*) of optical density, obtained after densitometric analysis of the bands corresponding to wild-type and mutant EGFP-Q2 divided by that of each respective α-tubulin band intensity. *C*, shows the same data of *panel B*, after normalization to the maximal value (24 h post-transfection) for each construct. In *B* and *C*, each data point is the mean ± S.E. calculated from five separate experiments. The *asterisks* denote values significantly different ($p < 0.05$) from respective controls.

Electrophysiological and Biochemical Analysis of KCNQ2 C-terminal Mutations Expressed Homomerically—To investigate the functional consequences of the 2043ΔT mutation in *Q2*, we incorporated this mutation into the EGFP-Q2 fusion construct (EGFP-Q2 2043ΔT). In addition, we also generated an EGFP fusion construct reproducing the sequence of another previously described BFNC-causing *Q2* mutation, namely a deletion of a *G* at position 2513 (EGFP-Q2 2513ΔG); this frameshift mutation led to the substitution of the last seven C-terminal amino acids of Q2 and to the incorporation of the same additional 56 residues incorporated by the 2043ΔT mutation (19).

Electrophysiological analysis of these two fusion constructs after 24–48 h post-transfection revealed that the EGFP-Q2 2043ΔT mutation failed to give rise to functional voltage-gated K$^+$ channels; on the other hand, EGFP-Q2 2513ΔG mutant subunits were able to produce significant amounts of K$^+$ currents, although these were smaller than those recorded from EGFP-Q2-transfected cells (Fig. 2, *A* and *B*).

Western blot experiments, performed with an anti-EGFP monoclonal antibody in cell lysates from wild-type- and 2043ΔT EGFP-Q2-transfected CHO cells at various times post-transfection (6, 12, 24, 34 and 48 h), revealed that the steady-state levels of EGFP-Q2 2043ΔT subunits were markedly reduced when compared with wild-type Q2 subunits at all times post-transfection (Fig. 3, *A* and *B*). After normalization to the maximum of the intensity values of the data shown in Fig. 3*B* for both EGFP-Q2 and EGFP-Q2 2043ΔT subunits, it was found that the cellular content of EGFP-Q2 mutant subunits declined faster than that of wild-type subunits with increasing times post-transfection (Fig. 3*C*). In fact, in the 24–34 h post-transfection interval, EGFP-Q2 subunit content decreased by <30%, whereas that of EGFP-Q2 2043ΔT mutant subunits was reduced by >70% (Fig. 3*C*). Similar data were also obtained when primary antibodies directed against an epitope in the N-terminal region of KCNQ2 subunits were used (data not shown). Interestingly, also EGFP-Q2 subunits carrying the 2513ΔG mutation showed a decreased expression at all time points, although the effect was not as dramatic as that shown for the 2043ΔT mutation; in three separate time-course experiments, the intensities of the bands corresponding to EGFP-Q2 2513ΔG subunits was 41.5 ± 3.6% of those of wild-type EGFP-Q2 subunits 48 h post-transfection ($p < 0.05$).

Effect of the 2043ΔT Mutation on KCNQ2 Subunit Stability—Several mechanisms might have been responsible for the dramatic reduction in the steady-state expression of EGFP-Q2 2043ΔT mutant subunits when
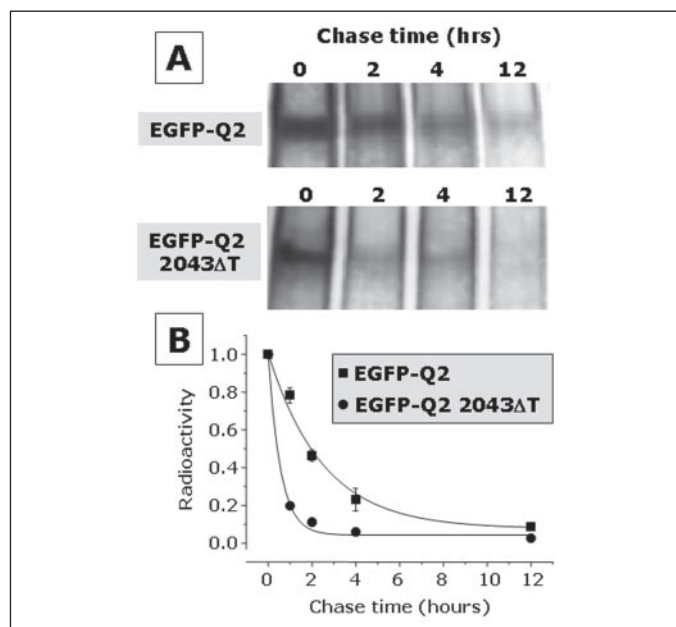
FIGURE 4. **Pulse-chase analysis of wild-type EGFP-Q2 and EGFP-Q2 2043ΔT mutant subunit stability.** *A*, representative images from autoradiographic films of experiments in CHO cells transfected with the indicated plasmids; metabolic labeling was performed for 30 min (60 min in some experiments) 24 h post-transfection, followed by chase times of 1, 2, 4, and 12 h. The data shown are representative of five separate experiments, each giving comparable results. *B*, densitometric quantification of the bands corresponding to EGFP-Q2 or EGFP-Q2 2043ΔT from data such as those shown in *A*, normalized to the value at times 0 (no chase times). Each data point is the mean ± S.E. calculated from five separate experiments.

compared with EGFP-Q2 subunits. Interestingly, fluorescent-activated cell sorter experiments revealed that the percent of CHO cells showing EGFP fluorescence above background was similar after transfection with EGFP-Q2 or EGFP-Q2 2043ΔT plasmids (33.4 ± 5.3% *versus* 29.3 ± 2.5%, respectively, $n = 4$; $p > 0.05$), ruling out possible differences in transfection efficiency as a possible explanation for the differences in subunit expression previously described in Western blot experiments. Furthermore, similar expression levels of EGFP-Q2 and EGFP-Q2 2043ΔT subunits were detected in an *in vitro* transcription-translation assay using reticulocyte lysates (data not shown). To directly test the hypothesis that the 2043ΔT mutation caused Q2 subunits to undergo faster degradation, as also suggested by the data of Fig. 3*B*, pulse-chase experiments in transiently transfected CHO cells were performed to compare the rate of disappearance of EGFP-Q2 2043ΔT subunits with that of EGFP-Q2 subunits. The results of these experiments revealed that the half-life of EGFP-Q2 subunits carrying the 2043ΔT mutation was 0.6 ± 0.1 h, four times shorter than that of wild-type EGFP-Q2 subunits (2.4 ± 0.2 h, $n = 4$, $p < 0.05$) (Fig. 4, *A* and *B*). Similar data were also observed in CHO cells stably transfected with wild-type and mutant constructs, suggesting therefore that the observed difference could not be accounted for by the transient transfection procedure (data not shown). Closer inspection to the data of Fig. 4*A* also showed that, at time 0 (when the cells were lysed immediately after the 30-min metabolic labeling pulse), the difference in intensity of the bands corresponding to EGFP-Q2 2043ΔT and EGFP-Q2 subunits was much less pronounced when compared with that revealed by the Western blot data of Fig. 3; this result seems consistent with the hypothesis that the shorter half-life of EGFP-Q2 2043ΔT subunits is largely responsible for the marked decrease in steady-state levels of these mutant subunits when compared with EGFP-Q2 subunits.

To investigate the possible involvement of the proteasomal degradative pathway in the enhanced degradation of Q2 subunits prompted by

the 2043ΔT mutation, we used the proteasomal inhibitor MG132 in Western blot experiments in CHO cells transfected with plasmids encoding for EGFP-Q2 or EGFP-Q2 2043ΔT subunits. Treatment with MG132 (20 μM) between 24 and 34 h post-transfection fully reversed the marked decrease of EGFP-Q2 2043ΔT subunits, whereas it did not affect the expression level of EGFP-Q2 subunits (Fig. 5, *A* and *B*). Noticeably, treatment of Q2 2043ΔT-transfected cells with MG132 failed to recover a significant fraction of functional voltage-gated K^+ channel subunits at the plasma membrane; in fact, the K^+ current density recorded at +20 mV from CHO cells transfected with the EGFP-Q2 2043ΔT plasmid and treated with MG132 was 1.28 ± 0.24 pA/pF ($n = 12$), a value that did not differ from that recorded in control EGFP-transfected cells (0.70 ± 0.21 pA/pF, $n = 12$).

Immunocytochemical Analysis of Wild-type and Mutant KCNQ2 Subunit Expression—To verify whether EGFP-Q2 2043ΔT subunits underwent an altered cellular processing, the subcellular distribution of these mutant subunits, as well as that of EGFP-Q2 2513ΔG subunits, was investigated by confocal immunofluorescence microscopy and their expression pattern was compared with that of EGFP-Q2 subunits. To this aim, we analyzed human hepatoma Huh-7-transfected cells, which are more flat and extended and thus more suitable for confocal analysis, and CHO cells (29). As shown in Fig. 6*A*, the majority of transiently expressed EGFP-Q2 subunits was distributed intracellularly and co-localized with the endoplasmic reticulum (ER) resident protein calreticulin. This is similar to what has been described in native neurons, where Q2 subunits are abundantly present in intracellular compartments (30, 31). Little EGFP-Q2 subunits were localized in the Golgi complex, as indicated by the lack of co-localization with the Golgi marker GM-130 (Fig. 6*B*). This result may suggest fundamental differences between the cellular processing of Q2 subunits and the K^+ channels subunits encoded by the human *Ether-a-gogo-Related* gene *1* (hERG1), which have been shown to interact with GM-130 in biochemical, morphological, and functional studies (32). Closer inspection to the data revealed a weak but convincing cell-surface labeling only in EGFP-Q2-transfected cells (as indicated by the *arrows*). In contrast, EGFP-Q2 2043ΔT subunits appeared not to be present on the cell surface and were mostly located in enlarged sub-regions of the ER (Fig. 6, *A* and *B*). Overall, the spatial organization of the ER in EGFP-Q2 2043ΔT-expressing cells appeared more irregular in comparison to EGFP-Q2-expressing cells or to untransfected cells (see calreticulin panels in Fig. 6*A*). A similarly altered distribution pattern, although less dramatic, was also observed with the EGFP-Q2 2513ΔG subunits (Fig. 6, *A* and *B*). Similar subcellular distribution patterns were obtained in CHO cells transfected with the same three plasmids (data not shown).

To improve the detection of plasma membrane-specific signals related to KCNQ2 subunit expression in non-permeabilized cells in immunocytochemical experiments, we engineered a cDNA construct whose expression led to the synthesis of EGFP-Q2 subunits, which carried an extracellular HA epitope (EGFP-Q2/HA). Homomeric assembly of EGFP-Q2/HA subunits gave rise to macroscopic K^+ currents identical in size and gating properties to those of the EGFP-Q2 subunits (Fig. 7*A*), suggesting therefore that the insertion of the HA epitope did not grossly alter subunit function. Furthermore, EGFP-Q2/HA subunit surface expression could be detected in transiently transfected CHO cells with a biochemical approach using biotinylation of membrane proteins (Fig. 7*B*). In addition, confocal immunofluorescence analysis showed an HA-related signal due to EGFP-Q2/HA subunits expression on the plasma membrane of non-permeabilized cells (Fig. 7*C*). Noticeably, the distribution of this

FIGURE 5. **Effect of the proteasomal inhibitor MG132 on EGFP-Q2 and EGFP-Q2 2043ΔT subunit expression levels.** *A*, representative Western blots showing the effect of MG132 treatment on EGFP-Q2 and EGFP-Q2 2043ΔT protein expression in total cell lysates from CHO cells; fusion proteins were detected using an anti-EGFP monoclonal antibody. CHO cells were transfected with plasmids encoding for EGFP-Q2 or EGFP-Q2 2043ΔT subunits in parallel 6-well plates; 24 h post-transfection, some plates were subjected to cell lysis, whereas in others MG132 (20 μM) or vehicle was added. After 10 h, the cells were lysed and the extracted proteins subjected to Western blot analysis. *B*, the intensity of the bands corresponding to EGFP-Q2 (*left panel*) or EGFP-Q2 2043ΔT subunits (*right panel*) was calculated by densitometric analysis and expressed as a function of that observed in cells lysed 24 h post transfection before drug treatment. Each bar is the mean ± S.E. of five different experiments. The *asterisk* denotes a value significantly different ($p < 0.05$) from respective control.
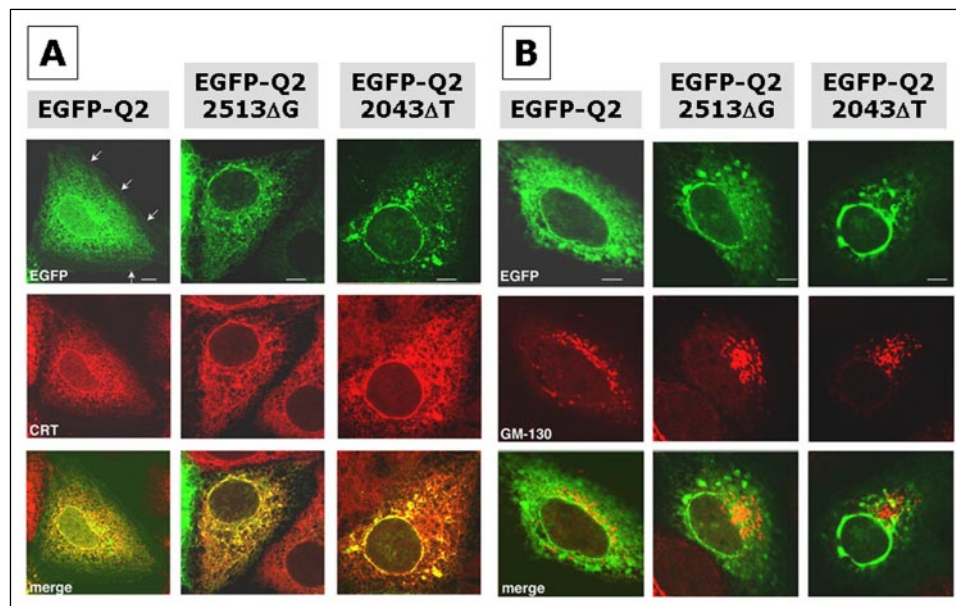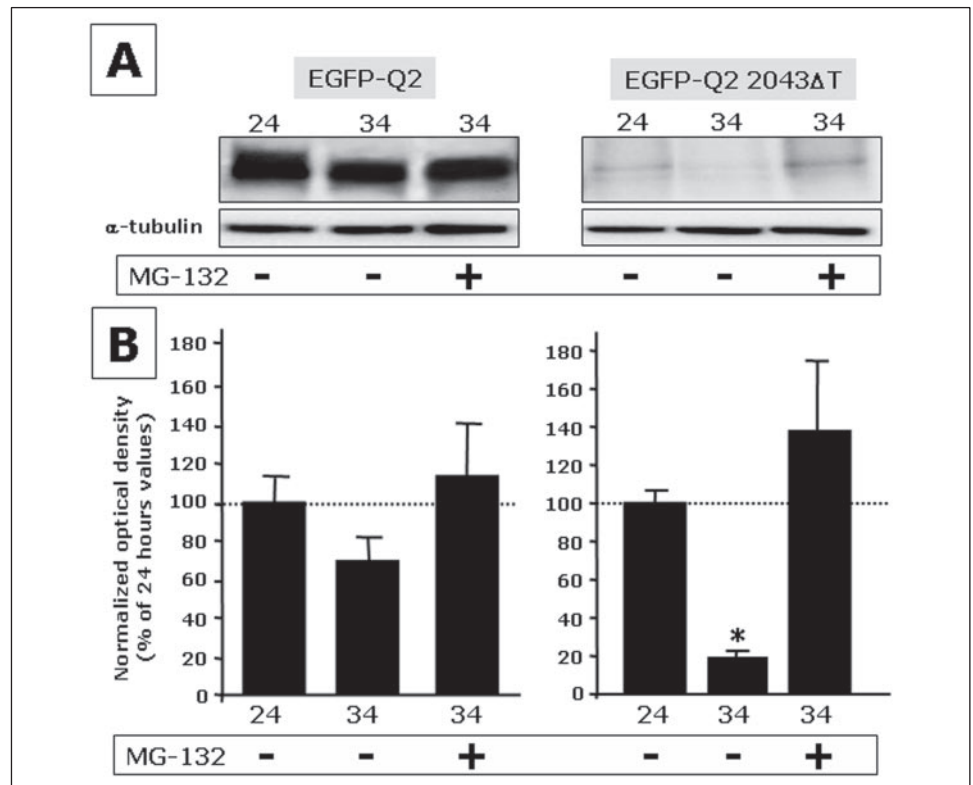
FIGURE 6. **Intracellular distribution of wild-type and mutant EGFP-Q2 subunits in Huh-7 cells.** Parallel cultures of Huh-7 cells grown on coverslips were transiently transfected to express the indicated EGFP-Q2 subunits. 24 h post-transfection the cells were fixed and processed for single section confocal immunofluorescence analysis. *Bar*, 5 μm. *CRT*, calreticulin. The *arrows* in *panel A* (EGFP-Q2 expressing cells) point to the plasma membrane.

surface signal appeared, for the most part, to be distinct from that of the EGFP-related fluorescence, which was mostly distributed intracellularly (Fig. 7*C*). On the other hand, EGFP-Q2/HA subunits carrying the 2043ΔT mutation were detected in total lysates (although reduced when compared with wtEGFP-Q2/HA subunits; Fig. 7*B*) but tested negative for voltage-gated K⁺ currents (Fig. 7*A*), and surface expression in both biotinylation assays (Fig. 7*B*) and immunofluorescence confocal analysis (Fig. 7*C*). As expected, permeabilization of CHO cells transfected with both EGFP-Q2/HA and EGFP-Q2/HA 2043ΔT plasmids revealed an intense intracellular signal with anti-HA antibodies whose distribution coincided with that of the EGFP-related signal (data not shown).

Heteromeric Expression of Wild-type and Mutant KCNQ2 Subunits with KCNQ3 Subunits—Co-expression of Q2 and Q3 subunits generate macroscopic currents much larger than those expected from simple summation of homomeric Q2 or Q3 currents. As shown in Figs. 8 (*A* and *B*), co-transfection of CHO cells with EGFP-Q2 and -Q3 plasmids led to a marked increase in macroscopic currents, suggesting that covalent linkage of the EGFP onto Q2 N terminus did not interfere with Q3-induced current potentiation. Interestingly, co-expression of Q3 and EGFP-Q2 2043ΔT subunits led to the appearance of detectable macroscopic voltage-gated K⁺ currents, whose amplitude, although smaller than that of EGFP-Q2/Q3 heteromers, was clearly above background and significantly different from homomeric currents formed by

Decreased KCNQ2 Subunit Stability and BFNC

FIGURE 7. **Electrophysiological, biochemical, and morphological analysis of wt and mutant EGFP-Q2/HA subunits.** *A*, patch clamp recordings from CHO cells transfected with the plasmids encoding for wtQ2-EGFP/HA and EGFP-Q2/HA 2043ΔT fusion proteins. Holding potential: -80 mV; step potentials from -100 to $+40$ mV, in 20-mV steps; test potential: 0 mV; return potential: -80 mV (the protocol is shown in the *inset*). *B*, Western blot experiments performed in total lysates (*Total*) or streptavidin-purified biotinylated plasma membrane proteins (*Surface*), from untransfected CHO cells (*lanes 1*) or from CHO cells transfected with the EGFP-Q2/HA (*lanes 2*) or the EGFP-Q2/HA 2043ΔT plasmid (*lanes 3*). Note that the absence of immunoreactivity to the intracellular protein α-tubulin (*lower blot*) suggests that plasma membrane proteins were selectively isolated by the biotinylation procedure. *C*, single section confocal analysis of non-permeabilized CHO cells transiently transfected with EGFP-Q2/HA and EGFP-Q2/HA 2043ΔT plasmids. Immunolabeling was performed as described under "Experimental Procedures." In EGFP-Q2/HA-transfected cells, but not in cells expressing EGFP-Q2/HA 2043ΔT subunits, please note peripheral staining of membrane surface with anti-HA antibodies, as opposed to the EGFP fluorescence mostly located intracellularly. *Bar*, 5 μm.
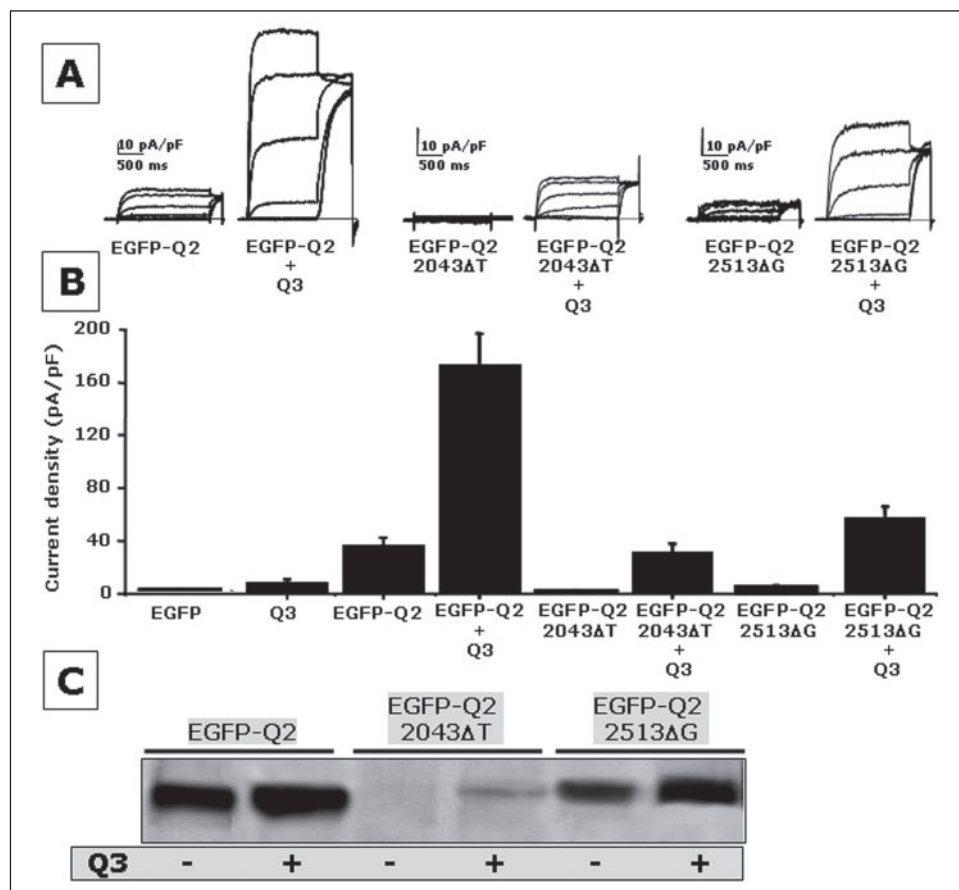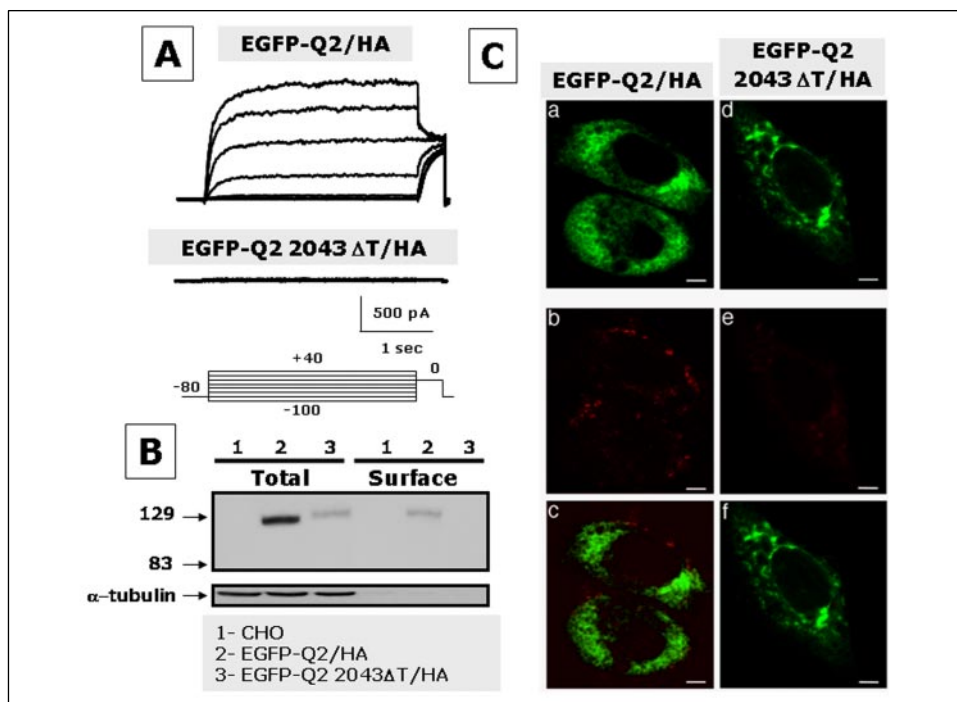

FIGURE 8. **Expression of C-terminal BFNC-causing KCNQ2 mutants in heteromeric configuration with KCNQ3 subunits.** *A*, representative patch clamp recordings from CHO cells transfected with the plasmids indicated. Holding potential: -80 mV; step potentials from -80 to $+20$ mV, in 20-mV steps; return potential: 0 mV. *B*, quantification of the current densities recorded from the experimental groups indicated. Each *bar* is the mean ± S.E. of 10–28 cells recorded from at least three different transfections. *C*, Western blot analysis of wild-type or mutant EGFP-Q2 subunit expression in isolated plasma membrane fractions from CHO cells transfected with EGFP-Q2, EGFP-Q2 2043ΔT, or EGFP-Q2 2513ΔG in the absence or in the presence of Q3, as indicated. Fusion proteins were detected using an anti-EGFP monoclonal antibody.

Q3 subunits. Interestingly, also the co-expression of EGFP-Q2 2513ΔG with Q3 subunits led to the expression of larger currents when compared with those formed by either subunits in homomeric configuration (Fig. 8, *A* and *B*).

Western blot experiments in plasma membrane fraction isolated after 24 h of transfection from CHO cells expressing EGFP-tagged Q2 wild-type or mutant subunits alone or together with Q3 subunits revealed that Q3 subunits expression doubled the steady-state amount

FIGURE 9. **Pharmacological and biophysical characterization of the currents recorded in CHO cells expressing different combinations of wild-type and mutant Q2 and Q3 subunits.** *A*, time course of the effects of 100 μM NEM on the currents recorded at 0 mV from cells transfected (24 h post-transfection) with the plasmids encoding for EGFP-Q2 (*triangles*), Q3 (*squares*), EGFP-Q2 plus Q3 (*circles*), and EGFP-Q2 2043ΔT plus Q3 (*diamonds*), as indicated. Peak current data at 0 mV for each pulse was recorded and expressed as a function of time, after normalization to the value recorded immediately before exposure to NEM. Each data point is the mean $\pm$ S.E. of five experiments. *B*, representative traces from CHO cells transfected (24 h post-transfection) with EGFP-Q2, Q3, EGFP-Q2 plus Q3, and EGFP-Q2 2043ΔT plus Q3, as indicated, before (*continuous line*) and after 10 min (*dotted lines*) of exposure to 100 μM NEM. Holding potential: -80 mV; test potential 0 mV. *C*, TEA blockade of the currents recorded from cells transfected with the plasmids encoding for EGFP-Q2 (*filled bars*), Q3 (*empty bars*), EGFP-Q2 plus Q3 (*fine hatched bars*), and EGFP-Q2 2043ΔT plus Q3 (*thick hatched bars*), as indicated. TEA sensitivity is expressed as percent of blockade of the currents recorded at 0 mV by perfusion for 3 min with 3 or 10 mM TEA, as indicated. Each data point is the mean $\pm$ S.E. of at least five different cells per experimental group. *D*, voltage dependence of activation of the currents recorded from cells transfected with EGFP-Q2 (*filled triangles*), Q3 (*filled squares*), EGFP-Q2 plus Q3 (*filled circles*), and EGFP-Q2 2043ΔT plus Q3 (*filled diamonds*), as indicated. Conductance-voltage curves were generated as indicated under "Experimental Procedures." Each data point is the mean $\pm$ S.E. of 7–12 cells recorded for each group in 3 different transfections.
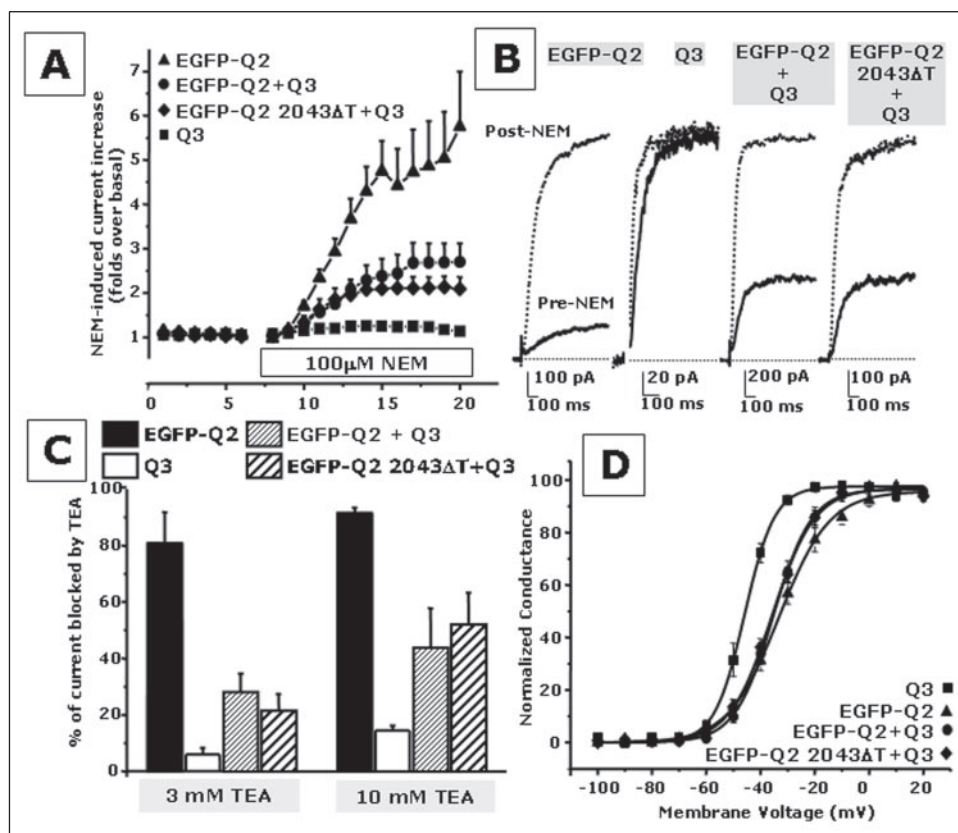
of wild-type EGFP-Q2 subunits (Fig. 8*C*). More importantly, plasma membrane expression of EGFP-Q2 2043ΔT subunits, which was not detectable when expressed in homomeric configuration, became detectable in heteromeric configuration with Q3. Interestingly, plasma-membrane expression of EGFP-Q2 2513ΔG subunits was also enhanced upon Q3 co-transfection (Fig. 8*C*).

When compared with homomeric Q3 channels, heteromeric channels incorporating both Q2 and Q3 subunits acquire an increased sensitivity to pharmacological modulation by activators such as *N*-ethylmaleimide (NEM) (33), and blockers such as tetraethylammonium (TEA) (5). To investigate whether functional heteromeric channels underlie the macroscopic K$^+$ currents recorded in cells co-transfected with Q3 and EGFP-Q2 2043ΔT plasmids, we investigated the pharmacological sensitivity to NEM and TEA of the currents recorded upon CHO cell expression of different subunit combinations. As shown in Fig. 9*A*, 100 μM NEM potently increased the macroscopic K$^+$ currents carried by homomeric EGFP-Q2 subunits, which, after 10–15 min of drug superfusion, were about 5 times larger than before NEM application; by contrast, 100 μM NEM failed to affect the maximal amplitude of the current carried by homomeric Q3 channels. Moreover, K$^+$ currents generated upon EGFP-Q2 plus Q3 co-transfection displayed an intermediate sensitivity to 100 μM NEM. Interestingly, macroscopic currents recorded from cells expressing both EGFP-Q2 2043ΔT and Q3 subunits displayed an NEM sensitivity comparable to that of heteromeric EGFP-Q2/Q3 channels, clearly distinct from Q3 homomeric channels (Fig. 9*A*). Fig. 9*B* shows representative K$^+$ current traces recorded at 0 mV from the four experimental groups before and after 100 μM NEM exposure. In addition, blockade by 3 and 10 mM TEA of the currents recorded from cells co-transfected with both EGFP-Q2 2043ΔT and Q3 plasmids was markedly enhanced when compared with that of

cells expressing only Q3 subunits; in fact, TEA sensitivity of the currents recorded from cells transfected with EGFP-Q2 2043ΔT and Q3 plasmids was indistinguishable from that of cells transfected with EGFP-Q2 and -Q3 plasmids (Fig. 9*C*).

Finally, when Q2 subunits were expressed in homomeric or heteromeric configurations, the resulting K$^+$ currents displayed a rightward shift in the midpoint potential and a less steep voltage dependence of the activation process when compared with those formed by homomeric Q3 channels. In CHO cells transfected with both EGFP-Q2 2043ΔT and Q3 plasmids, the voltage dependence of activation of the macroscopic currents was identical to that of heteromeric EGFP-Q2/Q3 channels and clearly distinct from that of homomeric Q3 channels (Fig. 9*D*). In fact, the $V_{1/2}$ and the k values for the activation curves were, respectively, -35.7 ± 0.4 mV and 7.8 ± 0.3 mV/e-fold for EGFP-Q2/Q3 ($n = 9$), -35.3 ± 0.2 mV and 7.1 ± 0.2 mV/e-fold for EGFP-Q2 2043ΔT/Q3 ($n = 7$), and -45.9 ± 0.2 mV and 5.5 ± 0.2 mV/e-fold for homomeric Q3 channels ($n = 11$).

To investigate whether Q3 subunits interfered with the stability of wild-type and mutant EGFP-Q2 subunits, we compared, by means of pulse-chase experiments, the rate of degradation of EGFP-Q2 and EGFP-Q2 2043ΔT subunits when expressed together with Q3 subunits (Fig. 10). The results of these experiments revealed that co-expression with Q3 subunits significantly reduced the degradation rate of EGFP-Q2 2043ΔT subunits; in fact, the half-life of EGFP-Q2 subunits carrying the 2043ΔT mutation went from 0.6 ± 0.1 h in the absence of Q3 subunits to 1.6 ± 0.3 h when co-transfected with Q3 subunits ($n = 3$, $p < 0.05$). Interestingly, Q3 subunits failed to affect the stability of EGFP-Q2 subunits; the half-life calculated from these experiments was 2.2 ± 0.4 h, a value that was similar to that obtained without Q3 subunit co-expression (2.4 ± 0.2 h) ($n = 3$, $p > 0.05$).
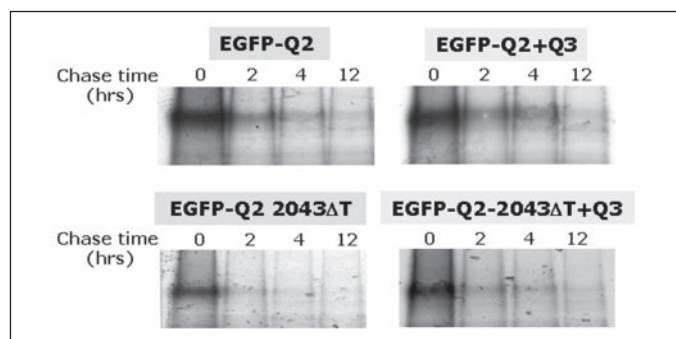
FIGURE 10. **Pulse-chase analysis of the effect of Q3 subunit co-expression on wild-type EGFP-Q2 and EGFP-Q2 2043ΔT mutant subunit stability.** Representative images from autoradiographic films of experiments in CHO cells transfected with the indicated plasmids; metabolic labeling was performed for 30 min (60 min in some experiments) 24 h post-transfection, followed by chase times of 1, 2, 4, and 12 h. The data shown are representative of three separate experiments, each giving comparable result.

DISCUSSION

The aim of the present study has been to clarify the molecular mechanism by which a BFNC-causing a single-base deletion (2043ΔT) in the gene encoding for Q2 subunits decreased I_{KM} function (26). The results obtained suggest that the 2043ΔT mutation reduces the steady-state cellular levels of Q2 subunits as a consequence of a marked enhancement of their degradation possibly occurring via the proteasomal disposition pathway. Furthermore, mutant Q2 subunits display a drastic reduction of their delivery to the plasma membrane. Co-expression with Q3 subunits at least partially reverses the enhanced degradation caused by the *Q2* 2043ΔT mutation, leading to the expression of functional heteromeric channels. Collectively, the present results suggest that mutation-induced enhanced degradation of Q2 subunits may represent a novel molecular mechanism causing epilepsy in neonates.

Functional Consequences of the EGFP-Q2 2043ΔT Mutation: Homomeric Expression—When the mutant protein was fused to the EGFP (EGFP-Q2 2043ΔT) and expressed in homomeric configuration in mammalian CHO cells, it failed to form functional channels, as previously shown for homomeric Q2 2043ΔT subunits expression in non-fusion constructs in CHO cells and *Xenopus* oocytes (26). Furthermore, Western blot analysis in isolated plasma-membrane fractions from transfected CHO cells failed to detect significant expression of the mutant protein and also revealed a marked decrease in the steady-state protein levels in total cell lysates analyzed at various times post-transfection. Pulse-chase experiments showed that, when expressed in homomeric form, EGFP-Q2 2043ΔT mutant subunits were degraded four times faster than wild-type EGFP-Q2 subunits; thus, a mutation-induced increased subunit disposal is at least in part responsible for the strong decrease of the steady-state content of EGFP-Q2 2043ΔT subunits in the total cell lysates.

Noticeably, these experiments provide a measure of wild-type Q2 half-life (2.4 h) that is within the ranges observed for some other ion channels subunits such as $K_v1.1$ (5 h) (34), hERG1 (8 h) (35), hIK1 (3.2 h) (36), and β and γ subunits of the amiloride-sensitive epithelial sodium channels (2 h) (37). Although most of these data have been obtained in heterologous expression systems, it has been speculated that these relatively short half-lives (when compared with other membrane proteins) provide greater flexibility for modulation and allow the cells to keep channel expression low in native tissues (34).

Mutation-induced altered regulation of protein degradation is a well known cause of disease. The present results with the Q2 2043ΔT muta-

tion bear some resemblance with those obtained with other disease-associated mutant proteins. In fact, cystic fibrosis transmembrane regulator chloride channel subunits carrying the ΔF508 mutation, the most common genetic defect causing cystic fibrosis in humans, have been shown to undergo an accelerated degradation as a consequence of a misfolding defect recognized by the ER quality control systems (38). Misfolded proteins undergo disposal by ER-associated degradation, being retro-translocated from the ER into the cytosol, where they may undergo proteasomal degradation (39); ΔF508 subunits appear to be mostly disposed via ER-associated degradation (40), although other non-proteasomal proteolytic systems may also contribute to their degradation. Similarly, the dominant-negative effects of the A561V mutation in hERG1 K^+ channels causing the inherited arrhythmia known as Long QT syndrome (LQTS-2) have been interpreted as a consequence of the ability of the mutant subunits to misfold assembling tetramers and to target them for early proteasomal degradation (35). Noticeably, the structural requirements for proteasomal degradation seem to be very stringent, as also suggested by the recent observation that different mutations in the voltage-sensing S_4 region may target $K_v1.1$ subunits to proteasomal or non-proteasomal disposal pathways (41). Our observation that the strong reduction in the steady-state levels of Q2 subunits carrying the 2043ΔT mutation, prompted by the enhanced subunit degradation, can be reversed by the proteasomal inhibitor MG132, raises the possibility that proteasomal disposition pathways may be an important mechanism for degradation of Q2 subunits carrying C-terminal mutations. This degradation mechanism seems to be specifically triggered by the mutation, because proteasomal inhibition failed to interfere with the disposal of wild-type Q2 subunits. However, it should be noticed that, even after exposure to MG132, the total cellular content of EGFP-Q2 2043ΔT subunits was still much lower than that of wild-type EGFP-Q2 subunits, and voltage-gated K^+ currents could not be recorded in electrophysiological experiments. These results suggest an extreme complexity of the molecular machinery controlling subunit surface expression. Nevertheless, the results obtained allow us to hypothesize that, in addition to permeation or gating defects affecting normally assembled channels (42), a reduced Q2 subunit stability also involving proteasomal degradation represents a novel pathogenetic mechanism for BFNC. Interestingly, the 2043ΔT mutation here investigated affects the distal part of the Q2 C terminus, a region where several BFNC-causing mutations cluster (17).

Functional Consequences of the EGFP-Q2 2043ΔT Mutation: Heteromeric Expression—Expression of Q2 with Q3 subunits produces a large increase in macroscopic current size, as also revealed by the present experiments upon co-expression of EGFP-Q2 and -Q3 subunits. This effect cannot be entirely accounted for by an increase of the single channel conductance or of the opening probability of the heteromeric channels (43), but also involves an enhanced surface expression of subunits (20, 44). In analogy to other heteromeric K^+ channels (45), it has been proposed that this enhanced expression may be due to yet unknown ER retention or export signals that may be hidden or uncovered by the interaction of Q2 and Q3 subunits. Intriguingly, while EGFP-Q2 2043ΔT mutant subunits failed to express on the plasma membrane and to form functional channels when expressed homomerically, the simultaneous expression with Q3 subunits allowed EGFP-Q2 2043ΔT mutant subunits to be detected on the plasma membrane. Furthermore, co-expression of EGFP-Q2 2043ΔT with Q3 subunits led to the appearance of significant voltage-gated macroscopic K^+ currents; these currents displayed a pharmacological sensitivity to the cysteine-modifying reagent NEM (33) and to the pore-blocked TEA (5) identical to those of

heteromeric channels composed of EGFP-Q2 and Q3 subunits. In addition, the voltage dependence of activation of the K$^+$ currents recorded from CHO cells co-expressing EGFP-Q2 2043ΔT and Q3 subunits was shifted toward more positive potentials when compared with that of homomeric channels composed of Q3 subunits; similar results were also observed in heteromeric channels composed of Q2 and Q3 subunits (42, 43). Altogether, the present results suggest that heteromeric channels composed of EGFP-Q2 2043ΔT and Q3 subunits are functional, thus providing support to the hypothesis that EGFP-Q2 2043ΔT mutant subunits fail to give rise to functional channels in homomeric configuration mainly as a consequence of an impaired subunit processing leading to a dramatic reduction of their export to the plasma membrane. Q3 subunits seem to at least partially restore the impaired processing of EGFP-Q2 2043ΔT subunits, as also revealed by the ability of Q3 subunits to increase the Q2 2043ΔT subunits half-life in pulse-chase experiments.

An highly conserved C-terminal domain in KCNQ-type subunits, the subunit interaction domain or *sid* (22, 46), corresponding to the region between amino acids 528 and 623 of the Q2 sequence, has been proposed to mediate the subunit specificity of KCNQ channel assembly and, possibly, the resulting enhanced expression of heteromeric channels. Our results show that the 2043ΔT mutation, which occurs at a site in Q2 C terminus downstream of the *sid* domain, allows the interaction between mutant Q2 and Q3 subunits, therefore supporting the hypothesis that this domain mediates the interaction between KCNQ-type subunits, which leads to the heteromeric current enhancement. Furthermore, the ability of Q3 subunits to rescue the mutation-induced enhanced degradation of Q2 2043ΔT subunits suggests that the interaction between Q2 and Q3 subunits is an early step in the biogenesis of Q2/Q3 heteromers and occurs before the ER-mediated misfolding recognition. This result bears an obvious relevance for the physiology of I$_{KM}$, which is thought to be primarily underlied by heteromeric assembly of these two subunits (5). Furthermore, the fact that Q2 2043ΔT subunits failed to exert dominant-negative effects when expressed with Q2/Q3 subunits (26) suggests haploinsufficiency as the primary mechanism for I$_{KM}$ deficit and BFNC pathogenesis in the affected family.

Genotype-Phenotype Correlations—The present results might provide clues on the genotype-phenotype correlations for some of the atypical clinical or electroencephalographic features associated in some families with BFNC. In fact, the proband affected by the 2043ΔT mutation in *Q2* developed a centrotemporal spike trait at the age of 3 years, well before the mean age of appearance of 7 years in families not affected by BFNC (26); in another recently described mutation in Q2 C terminus (1931ΔG), located close to the 2043ΔT mutation, the age of remission (12–18 months) was delayed when compared with most BFNC patients (3–6 months) (47). On the other hand, the more distal 2513ΔG mutation in *Q2* produced less dramatic functional consequences, because patients affected by this mutation only showed classic BFNC, with no atypical clinico-electrophysiological features after the BFNC symptoms disappeared (19). Therefore, one might speculate that *Q2* mutations affecting more distal sites in the C terminus prompt less dramatic consequences on neuronal excitability, being thus associated with milder clinical phenotypes.

REFERENCES

1. Shieh, C.-C., Coghlan, M., Sullivan, J. P., and Gopalakrishnan, M. (2000) *Pharmacol. Rev.* **52,** 557–593
2. Brown, D. A., and Adams, P. R. (1980) *Nature* **283,** 673–676
3. Rogawski, M. A. (2000) *Trends Neurosci.* **23,** 393–398
4. Marrion, N. V. (1997) *Annu. Rev. Physiol.* **59,** 483–504
5. Wang, H. S., Pan, Z., Shi, W., Brown, B. S., Wymore, R. S., Cohen, I. S., Dixon, J. E., and McKinnon, D. (1998) *Science* **282,** 1890–1893
6. Cooper, E. C., Aldape, K. D., Abosch, A., Barbaro, N. M., Berger, M. S., Peacock, W. S., Jan, Y. N., and Jan, L. Y. (2000) *Proc. Natl. Acad. Sci. U. S. A.* **97,** 4914–4919
7. Kubisch, C., Schroeder, B. C., Friedrich, T., Lutjohann, B., El-Amraoui, A., Marlin, S., Petit, C., and Jentsch, T. J. (2000) *Cell* **96,** 437–446
8. Lerche, C., Scherer, C. R., Seebohm, G., Derst, C., Wei, A. D., Busch, A. E., and Steinmeyer, K. (2000) *J. Biol. Chem.* **275,** 22395–22400
9. Schroeder, B. C., Hechenberger, M., Weinreich, F., Kubisch, C., and Jentsch, T. J. (2000) *J. Biol. Chem.* **275,** 24089–24095
10. Singh, N. A., Charlier, C., Stauffer, D., DuPont, B. R., Leach, R. J., Melis, R., Ronen, G. M. Bjerre, I., Quattlebaum, T., Murphy, J. V., McHarg, M. L., Gagnon, D., Rosales, T. O., Peiffer, A., Anderson, V. E., and Leppert, M. (1998) *Nat. Genet.* **18,** 25–29
11. Biervert, C., Schroeder, B. C., Kubisch, C., Berkovic, S. F., Propping, P., Jentsch, T. J., and Steinlein, O. K. (1998) *Science* **279,** 403–406
12. Charlier, C., Singh, N. A., Ryan, S. G., Lewis, T. B., Reus, B. E., Leach, R. J., and Leppert, M. (1998) *Nat. Genet.* **18,** 53–55
13. Steinlein, O. K. (1998) *Clin. Genet.* **54,** 169–174
14. Ronen, G. M., Rosales, T. O., Connolly, M., Anderson, V. E., and Leppert, M. (1993) *Neurology* **43,** 1355–1360
15. Steinlein, O.K., Stoodt, J., Biervert, C., Janz, D., and Sander, T. (1999) *Neuroreport* **10,** 1163–1166
16. Haug, K., Hallmann, K., Horvath, S., Sander, T., Kubisch, C., Rau, B., Dullinger, J., Beyenburg, S., Elger, C.E., Propping, P., and Heils. A. (2000) *Epilepsy Res.* **42,** 57–62
17. Singh, N. A., Westenskow, P., Charlier, C., Pappas, C., Leslie, J., Dillon, J., Anderson, V. E., Sanguinetti, M. C., and Leppert, M. F. (2003) *Brain* **126,** 2726–2737
18. Schroeder, B. C., Kubisch, C., Stein, V., and Jentsch, T. J. (1998) *Nature* **396,** 687–690
19. Lerche, H., Biervert, C., Alekov, A. K., Schleithoff, L., Lindner, M., Klinger, W., Bretschneider, F., Mitrovic, N., Jurkat-Rott, K., Bode, H., Lehmann-Horn, F., and Steinlein, O. K. (1999) *Ann. Neurol.* **46,** 305–312
20. Schwake, M., Pusch, M., Kharkovets, T., and Jentsch, T. J. (2000) *J. Biol. Chem.* **275,** 13343–13348
21. Dedek, K., Kunath, B., Kananura, C., Reuner, U., Jentsch, T. J., and Steinlein, O. K. (2001) *Proc. Natl. Acad. Sci. U. S. A.* **98,** 12272–12277
22. Schwake, M., Jentsch, T. J., and Friedrich, T. (2003) *EMBO Rep.* **4,** 76–81
23. Wen, H., and Levitan, I. B. (2002) *J. Neurosci.* **22,** 7991–8001
24. Yus-Najera, E., Santana-Castro, I., and Villarroel, A. (2002) *J. Biol. Chem.* **277,** 28545–28553
25. Hoshi, N., Zhang, J. S., Omaki, M., Takeuchi, T., Yokoyama, S., Wanaverbecq, N., Langeberg, L. K., Yoneda, Y., Scott, J. D., Brown, D. A., and Higashida, H. (2003) *Nat. Neurosci.* **6,** 564–571
26. Coppola, G., Castaldo, P., Miraglia del Giudice, E., Bellini, G., Galasso, F., Soldovieri, M. V., Anzalone, L., Sferro, C., Annunziato, L., Pascotto, A., and Taglialatela, M. (2003) *Neurology* **61,** 131–134
27. Borgatti, R., Zucca, C., Cavallini, A., Ferrario, M., Panzeri, C., Castaldo, P., Soldovieri, M. V., Baschirotto, C., Bresolin, N., Dalla Bernardina, B., Taglialatela, M., and Bassi M. T. (2004) *Neurology* **63,** 57–65
28. Bonatti, S., Migliaccio, G., and Simons, K. (1989) *J. Biol. Chem.* **264,** 12590–12595
29. Mottola, G., Jourdan, N., Castaldo, G., Malagolini, N., Lahm, A., Serafini-Cessi, F., Migliaccio, G., and Bonatti, S. (2000) *J. Biol. Chem.* **275,** 24070–24079
30. Shah, M.M., Mistry, M., Marsh, S.J., Brown, D.A., and Delmas, P. (2002) *J. Physiol.* **544,** 29–37
31. Peretz, A., Degani, N., Nachman, R., Uziyel, Y., Gibor, G., Shabat, D., and Attali, B. (2005) *Mol. Pharmacol.* **67,** 1053–1066
32. Roti, E. C., Myers, C. D., Ayers, R. A., Boatman, D. E., Delfosse, S. A., Chan, E. K., Ackerman, M. J., January, C. T., and Robertson, G. A. (2002) *J. Biol. Chem.* **277,** 47779–47785
33. Li, Y., Gamper, N., and Shapiro, M. S. (2004) *J. Neurosci.* **24,** 5079–5090
34. Deal, K. K., Lovinger, D. M., and Tamkun, M. M. (1994) *J. Neurosci.* **14,** 1666–1676
35. Kagan, A., Yu, Z., Fishman, G. I., and McDonald, T. V. (2000) *J. Biol. Chem.* **275,** 11241–11248
36. Jones, H. M., Hamilton, K. L., Papworth, G. D., Syme, C. A., Watkins, S. C., Bradbury, N. A., and Devor, D. C. (2004) *J. Biol. Chem.* **279,** 15531–15540
37. Malik, B., Schlanger, L., Al-Khalili, O., Bao, H. F., Yue, G., Price, S. R., Mitch, W. E., and Eaton, D. C. (2001) *J. Biol. Chem.* **276,** 12903–12910
38. Ward, C. L., Omura, S., and Kopito, R. R. (1995) *Cell* **83,** 121–127
39. Ellgaard, L., and Helenius, A. (2003) *Nat. Rev. Mol. Cell. Biol.* **4,** 181–191
40. Gelman, M. S., Kannegaard, E. S., and Kopito, R. R. (2002) *J. Biol. Chem.* **277,** 11709–11714

41. Myers, M. P., Khanna, R., Lee, E. J., and Papazian, D. M. (2004) *FEBS Lett.* **568,** 110–116

42. Castaldo, P., del Giudice, E. M., Coppola, G., Pascotto, A., Annunziato, L., and Taglialatela, M. (2002) *J. Neurosci.* **22,** RC199

43. Selyanko, A. A., Hadley, J. K., and Brown, D. A. (2001) *J. Physiol.* **534,** 15–24

44. Etxeberria, A., Santana-Castro, I., Regalado, M. P., Aivar, P., and Villarroel, A. (2004) *J. Neurosci.* **24,** 9146–9152

45. Zerangue, N., Schwappach, B., Jan, Y. N., and Jan, L. Y (1999) *Neuron* **22,** 537–548

46. Maljevic, S., Lerche, C., Seebohm, G., Alekov, A. K., Busch, A. E., and Lerche, H. (2003) *J. Physiol.* **548,** 353–360

47. Tang, B., Li, H., Xia, K., Jiang, H., Pan, Q., Shen, L., Long, Z., Zhao, G., and Cai, F. (2004) *J. Neurol. Sci.* **221,** 31–34

Decreased Subunit Stability as a Novel Mechanism for Potassium Current Impairment by a KCNQ2 C Terminus Mutation Causing Benign Familial Neonatal Convulsions

Maria Virginia Soldovieri, Pasqualina Castaldo, Luisa Iodice, Francesco Miceli,
Vincenzo Barrese, Giulia Bellini, Emanuele Miraglia del Giudice, Antonio Pascotto,
Stefano Bonatti, Lucio Annunziato and Maurizio Taglialatela

Access the most updated version of this article at doi: 10.1074/jbc.M510980200

Alerts:

- When this article is cited
- When a correction for this article is posted

Click here to choose from all of JBC's e-mail alerts

This article cites 47 references, 26 of which can be accessed free at
http://www.jbc.org/content/281/1/418.full.html#ref-list-1